arXiv:cond-mat/0305232v2 [cond-mat.str-el] 2 Jun 2003

Unusual charge transport and spin response of doped bilayer triangular antiferromagnets

Ying Liang and Tianxing Ma
Department of Physics, Beijing Normal University, Beijing 100875, China

Shiping Feng
Department of Physics, Beijing Normal University, Beijing 100875, China
Interdisciplinary Center of Theoretical Studies, Chinese Academy of Sciences, Beijing 100080, China
National Laboratory of Superconductivity, Chinese Academy of Sciences, Beijing 100080, China
(Received December 16, 2002)

Within the t-J model, the charge transport and spin response of the doped bilayer triangular antiferromagnet are studied by considering the bilayer interaction. Although the bilayer interaction leads to the band splitting in the electronic structure, the qualitative behaviors of the physical properties are the same as in the single layer case. The conductivity spectrum shows the low-energy peak and unusual midinfrared band, the temperature dependent resistivity is characterized by the nonlinearity metallic-like behavior in the higher temperature range, and the deviation from the metallic-like behavior in the lower temperature range, and the commensurate neutron scattering peak near the half-filling is split into six incommensurate peaks in the underdoped regime, with the incommensurability increases with the hole concentration at lower dopings, and saturates at higher dopings.

74.20.Mn, 74.25.Fy, 75.25.+z

I. INTRODUCTION

It has become clear in the past ten years that the most remarkable expression of the nonconventional physics of doped cuprates is found in the normal-state[1,2]. These unusual normal-state properties are due to the special microscopic conditions: (1) Cu ions situated in a square-planar arrangement and bridged by oxygen ions (CuO_2 plane), (2) weak coupling between neighboring layers, and (3) doping in such a way that the Fermi level lies near the middle of the Cu-O σ^* bond, where *one common feature* is the *square-planar* Cu arrangement[1,2]. In the underdoped and optimally doped regimes, it has been shown from the transport experiments[1,3] that the ratio of the c-axis and in-plane resistivity $R = \rho_c(T)/\rho_{ab}(T)$ ranges from $R \sim 100$ to $R > 10^5$, this reflects that the charged carriers are tightly confined to the CuO_2 planes. This large magnitude of the resistivity anisotropy also leads to the general notion that the physics of these materials is almost entirely two-dimensional (2D), and can be well described by a single CuO_2 plane[4]. However, this physical picture seems to be incompatible with the fact that the superconducting transition temperature T_c is closely related to the number of CuO_2 planes per unit cell, with single layer materials of a family generically having lower T_c than bilayer or trilayer materials[1,2]. Furthermore, some essential differences of the magnetic behaviors between doped single layer and bilayer cuprates have been found[5,6]. In the underdoped regime, it has been shown from the experiments that only incommensurate neutron scattering peaks for the single layer lanthanum cuprate are observed[5], however, both low-energy incommensurate neutron scattering peaks and high-energy commensurate $[\pi,\pi]$ resonance for the bilayer yttrium cuprate in the normal state are detected[6]. These experimental results highlight the importance of some sort of coupling between the CuO_2 planes within a unit cell. On the other hand, the bilayer band splitting in the doped bilayer cuprates was shown by the band calculation[7], and clearly observed[8] recently by the angle-resolved-photoemission spectroscopy in the underdoped and overdoped bilayer cuprates. This bilayer band splitting is due to a nonvanishing intracell coupling. Moreover, the magnitude of the bilayer splitting is constant over a large range of dopings[9].

However, many materials with the Cu arrangements on 2D non-square lattices have been synthetized[10–12]. In particular, it has been found from the experiments that there is a class of doped cuprates, $RCuO_{2+\delta}$, R being a rare-earth element, where the Cu ions are not arranged on a square-planar, but on a *triangular-planar lattice*[10], therefore allowing a test of the geometry effect on the normal-state properties, while retaining some other unique special microscopic features of the Cu-O bond. Since the strong electron correlation is common for both doped square and triangular antiferromagnets, it is expected that the unconventional normal-state properties existing in the doped square antiferromagnet may also be seen in the doped triangular antiferromagnet. However, within the t-J model, we[13,14] have discussed the charge transport and spin response of the doped single layer triangular antiferromagnet in the underdoped regime, and found that the normal-state properties of the doped single layer triangular lattice antiferromagnet are much different from these of the doped single layer square lattice antiferromagnet since the strong geometry effect in the triangular lattice system. The conductivity spectrum shows the unusual behavior at low energies and

anomalous midinfrared band separated by the charge-tranfer gap, in contrast with the doped square lattice antiferromagnet, the resistivity exhibits a nonlinearity in temperatures, and the commensurate neutron scattering peak near the half-filling is split into six incommensurate scattering peaks away from the half-filling. Considering these highly unusual charge transport and spin response in the underdoped regime, a natural question is what is the effect of the intracell coupling on the charge transport and spin response of the doped bilayer triangular antiferromagnet. On the other hand, the undoped bilayer triangular antiferromagnet is a good candidate for a 2D quantum system with the resonating valence bond spin liquid due to the strong geometry spin frustration and quantum interference effect between the layers[15]. This spin liquid state would be particularly attractive, given the intensive work on the spin liquid states on the square lattice, especially in connection with the superconductivity of doped cuprates[4]. Moreover, it has been shown that the doped and undoped triangular antiferromagnets present a pairing instability in an unconventional channel[16]. In this paper, we apply the fermion-spin theory[17] to study the charge transport and spin response of the doped bilayer triangular antiferromagnet. We hope that the information from the present work may induce further experimental works in doped antiferromagnets on the non-square lattice.

The paper is organized as follows. The theoretical framework is presented in Sec. II, where the single-particle holon and spinon Green's functions are calculated based on the t-J model by considering the bilayer interaction. Within this theoretical framework, we discuss the charge transport of the doped bilayer triangular antiferromagnet in Sec. III. It is shown that the conductivity spectrum shows a low-energy peak and unusual midinfrared band, while the temperature dependent resistivity is characterized by the nonlinearity metallic-like behavior in the higher temperature range, and the deviation from the metallic-like behavior in the lower temperature range. In Sec. IV, the spin response of the doped bilayer triangular antiferromagnet is studied. Our result shows that the commensurate neutron scattering peak near the half-filling is split into six incommensurate peaks in the underdoped regime, where the incommensurability is doping dependent, and increases with the hole concentration at lower dopings, and saturates at higher dopings. Sec. V is devoted to a summary and discussions. Our results also show that although the bilayer interaction leads to the band splitting in the electronic structure, the qualitative behavior of the charge transport and spin response are the same as in the single layer case[13,14].

II. THEORETICAL FRAMEWORK

As in the doped single layer triangular antiferromagnet[4,16], the essential physics of the doped bilayer triangular antiferromagnet is well described by the bilayer t-J model on the triangular lattice, and can be expressed as,

$$\begin{aligned} H = & -t_{\parallel}\sum_{ai\hat{\eta}\sigma} C^{\dagger}_{ai\sigma}C_{ai+\hat{\eta}\sigma} - t_{\perp}\sum_{i\sigma}(C^{\dagger}_{1i\sigma}C_{2i\sigma} + \text{h.c.}) \\ & - \mu\sum_{ai\sigma} C^{\dagger}_{ai\sigma}C_{ai\sigma} + J_{\parallel}\sum_{ai\hat{\eta}} \mathbf{S}_{ai}\cdot\mathbf{S}_{ai+\hat{\eta}} \\ & + J_{\perp}\sum_{i}\mathbf{S}_{1i}\cdot\mathbf{S}_{2i}, \end{aligned} \tag{1}$$

where the summation within the plane is over all sites i, and for each i, over its nearest-neighbor $\hat{\eta}$, $a = 1$, 2 is plane indices, $C^{\dagger}_{ai\sigma}$ ($C_{ai\sigma}$) is the electron creation (annihilation) operator, $\mathbf{S}_{ai} = C^{\dagger}_{ai}\vec{\sigma}C_{ai}/2$ are spin operators with $\vec{\sigma} = (\sigma_x, \sigma_y, \sigma_z)$ as Pauli matrices, and μ is the chemical potential. The bilayer t-J model (1) is supplemented by the single occupancy local constraint $\sum_{\sigma} C^{\dagger}_{ai\sigma}C_{ai\sigma} \leq 1$. This local constraint reflects the strong electron correlation in the doped antiferromagnet, and can be treated *properly in analytical form* within the fermion-spin theory[17] based on the charge-spin separation,

$$C_{ai\uparrow} = h^{\dagger}_{ai}S^{-}_{ai}, \quad C_{ai\downarrow} = h^{\dagger}_{ai}S^{+}_{ai}, \tag{2}$$

with the spinless fermion operator h_{ai} keeps track of the charge (holon), while the pseudospin operator S_{ai} keeps track of the spin (spinon), and then the low-energy behavior of the bilayer t-J model (1) can be rewritten in the fermion-spin representation as,

$$\begin{aligned} H = & t_{\parallel}\sum_{ai\hat{\eta}} h^{\dagger}_{ai+\hat{\eta}}h_{ai}(S^{+}_{ai}S^{-}_{ai+\hat{\eta}} + S^{-}_{ai}S^{+}_{ai+\hat{\eta}}) \\ & + t_{\perp}\sum_{i}(h^{\dagger}_{1i}h_{2i} + h^{\dagger}_{2i}h_{1i})(S^{+}_{1i}S^{-}_{2i} + S^{-}_{1i}S^{+}_{2i}) \\ & + \mu\sum_{ai} h^{\dagger}_{ai}h_{ai} + J_{\parallel\text{eff}}\sum_{ai\hat{\eta}}\mathbf{S}_{ai}\cdot\mathbf{S}_{ai+\hat{\eta}} \\ & + J_{\perp\text{eff}}\sum_{i}\mathbf{S}_{1i}\cdot\mathbf{S}_{2i}, \end{aligned} \tag{3}$$

where S^{+}_{ai} (S^{-}_{ai}) is the pseudospin raising (lowering) operator, $J_{\parallel\text{eff}} = J_{\parallel}[(1-x)^2 - \phi^2_{\parallel}]$, $J_{\perp\text{eff}} = J_{\perp}[(1-x)^2 - \phi^2_{\perp}]$, x is the hole doping concentration, and $\phi_{\parallel} = \langle h^{\dagger}_{ai}h_{ai+\hat{\eta}}\rangle$ and $\phi_{\perp} = \langle h^{\dagger}_{1i}h_{2i}\rangle$ are the holon particle-hole order parameters. The spinon and holon may be separated at the mean-field (MF) level, but they are strongly coupled beyond the MF approximation due to the strong holon-spin interaction.

In the bilayer system, because there are two coupled planes, then the energy spectrum has two branches. In

this case, the one-particle holon and spinon Green's functions are matrices, and are expressed as,

$$D(i-j,\tau-\tau') = D_L(i-j,\tau-\tau') + \sigma_x D_T(i-j,\tau-\tau'), \quad (4a)$$

$$g(i-j,\tau-\tau') = g_L(i-j,\tau-\tau') + \sigma_x g_T(i-j,\tau-\tau'), \quad (4b)$$

respectively, where the longitudinal and transverse parts are defined as,

$$D_L(i-j,\tau-\tau') = -\langle T_\tau S^+_{ai}(\tau) S^-_{aj}(\tau')\rangle, \quad (5a)$$

$$g_L(i-j,\tau-\tau') = -\langle T_\tau h_{ai}(\tau) h^\dagger_{aj}(\tau')\rangle, \quad (5b)$$

$$D_T(i-j,\tau-\tau') = -\langle T_\tau S^+_{ai}(\tau) S^-_{a'j}(\tau')\rangle, \quad (5c)$$

$$g_T(i-j,\tau-\tau') = -\langle T_\tau h_{ai}(\tau) h^\dagger_{a'j}(\tau')\rangle, \quad (5d)$$

with $a \neq a'$. At the half-filling, the bilayer t-J model (3) is reduced as the bilayer antiferromagnetic Heisenberg model. It has been shown[18] that as in the square lattice, there is indeed the antiferromagnetic long-range-order (AFLRO) in the ground state of the single layer triangular antiferromagnetic Heisenberg model, but this AFLRO is destroyed more rapidly with increasing dopings than on the square lattice due to the strong geometry frustration. Since the quantum interference effect between the layers in the bilayer triangular antiferromagnet does not favor the magnetic order for spins, then AFLRO in the doped bilayer triangular antiferromagnet is suppressed more fastly than the doped single layer antiferromagnet, therefore away from the half-filling, there is no AFLRO for the doped bilayer triangular antiferromagnet, *i.e.*, $\langle S^z_{ai}\rangle = 0$. Within the fermion-spin formalism, the MF theory of the doped square antiferromagnet in the underdoped and optimally doped regimes without AFLRO has been developed[19]. Following thier discussions, the MF holon and spinon Green's functions of the doped bilayer triangular antiferromagnet are obtained as,

$$g^{(0)}_L(k,\omega) = \frac{1}{2}\sum_{\nu=1,2}\frac{1}{\omega-\xi^{(\nu)}_k}, \quad (6a)$$

$$g^{(0)}_T(k,\omega) = \frac{1}{2}\sum_{\nu=1,2}(-1)^{\nu+1}\frac{1}{\omega-\xi^{(\nu)}_k}, \quad (6b)$$

$$D^{(0)}_L(k,\omega) = \frac{1}{2}\sum_{\nu=1,2}\frac{B^{(\nu)}_k}{\omega^2-(\omega^{(\nu)}_k)^2}, \quad (6c)$$

$$D^{(0)}_T(k,\omega) = \frac{1}{2}\sum_{\nu=1,2}(-1)^{\nu+1}\frac{B^{(\nu)}_k}{\omega^2-(\omega^{(\nu)}_k)^2}, \quad (6d)$$

respectively, where $B^{(\nu)}_k = \lambda[(2\epsilon_\parallel\chi^z_\parallel+\chi_\parallel)\gamma_k - (\epsilon_\parallel\chi_\parallel + 2\chi^z_\parallel)] - J_{\perp\rm eff}[\chi_\perp + 2\chi^z_\perp(-1)^\nu][\epsilon_\perp + (-1)^\nu]$, $\lambda = 2ZJ_{\parallel\rm eff}$, $\epsilon_\parallel = 1+2t_\parallel\phi_\parallel/J_{\parallel\rm eff}$, $\epsilon_\perp = 1+4t_\perp\phi_\perp/J_{\perp\rm eff}$, $\gamma_k = [\cos k_x + 2\cos(k_x/2)\cos(\sqrt{3}k_y/2)]/3$, and Z is the number of the nearest neighbor sites within the plane, while the MF holon and spinon excitation spectra are given by,

$$\xi^{(\nu)}_k = 2Zt_\parallel\chi_\parallel\gamma_k + 2\chi_\perp t_\perp(-1)^{\nu+1} + \mu, \quad (7a)$$

$$(\omega^{(\nu)}_k)^2 = A_1\gamma^2_k + A_2\gamma_k + A_3 + (-1)^{\nu+1}(X_1\gamma_k + X_2), \quad (7b)$$

with

$$A_1 = \alpha\epsilon_\parallel\lambda^2(\frac{1}{2}\chi_\parallel + \epsilon_\parallel\chi^z_\parallel), \quad (8a)$$

$$A_2 = \epsilon_\parallel\lambda^2[(1-Z)\alpha\frac{1}{Z}(\frac{1}{2}\epsilon_\parallel\chi_\parallel + \chi^z_\parallel) - \alpha(C^z_\parallel + \frac{1}{2}C_\parallel) - \frac{1}{2Z}(1-\alpha)] - \alpha\lambda J_{\perp\rm eff}[\epsilon_\parallel(C^z_\perp + \chi^z_\perp) + \frac{1}{2}\epsilon_\perp(C_\perp + \epsilon_\parallel\chi_\perp)], \quad (8b)$$

$$A_3 = \lambda^2[\alpha(C^z_\parallel + \frac{1}{2}\epsilon^2_\parallel C_\parallel) + \frac{1}{4Z}(1-\alpha)(1+\epsilon^2_\parallel) - \alpha\epsilon_\parallel\frac{1}{Z}(\frac{1}{2}\chi_\parallel + \epsilon_\parallel\chi^z_\parallel)] + \alpha\lambda J_{\perp\rm eff}[\epsilon_\parallel\epsilon_\perp C_\perp + 2C^z_\perp] + \frac{1}{4}J^2_{\perp\rm eff}(\epsilon^2_\perp + 1), \quad (8c)$$

$$X_1 = \alpha\lambda J_{\perp\rm eff}[\frac{1}{2}(\epsilon_\perp\chi_\parallel + \epsilon_\parallel\chi_\perp) + \epsilon_\parallel\epsilon_\perp(\chi^z_\perp + \chi^z_\parallel)], \quad (8d)$$

$$X_2 = -\alpha\lambda J_{\perp\rm eff}[\frac{1}{2}\epsilon_\parallel\epsilon_\perp\chi_\parallel + \epsilon_\perp(\chi^z_\parallel + C^z_\perp) + \frac{1}{2}\epsilon_\parallel C_\perp] - \epsilon_\perp J^2_{\perp\rm eff}/2, \quad (8e)$$

where the spinon correlation functions $\chi_\parallel = \langle S^+_{ai}S^-_{ai+\hat\eta}\rangle$, $\chi^z_\parallel = \langle S^z_{ai}S^z_{ai+\hat\eta}\rangle$, $\chi_\perp = \langle S^+_{1i}S^-_{2i}\rangle$, $\chi^z_\perp = \langle S^z_{1i}S^z_{2i}\rangle$, $C_\parallel = (1/Z^2)\sum_{\hat\eta\hat\eta'}\langle S^+_{ai+\hat\eta}S^-_{ai+\hat\eta'}\rangle$, $C^z_\parallel = (1/Z^2)\sum_{\hat\eta\hat\eta'}\langle S^z_{ai+\hat\eta}S^z_{ai+\hat\eta'}\rangle$, $C_\perp = (1/Z)\sum_{\hat\eta}\langle S^+_{2i}S^-_{1i+\hat\eta}\rangle$, and $C^z_\perp = (1/Z)\sum_{\hat\eta}\langle S^z_{1i}S^z_{2i+\hat\eta}\rangle$. In order to satisfy the sum rule for the correlation function $\langle S^+_{ai}S^-_{ai}\rangle = 1/2$ in the absence of AFLRO, a decoupling parameter α has been introduced in the MF calculation, which can be regarded as the vertex correction[19]. As a result of self-consistent motion of holons and spinons, all these mean-field order parameters, decoupling parameter, and the chemical potential are determined self-consistently.

In this paper we hope to discuss the optical, transport, and magnetic properties of the doped bilayer triangular antiferromagnet, then the second-order corrections for holons and spinons due to the holon-spinon interaction are necessary for the proper description of the holon motion in the background of the magnetic fluctuation and spinon motion in the background of the charged holon fluctuation. Within the fermion-spin theory, the full holon and spinon Green's functions of the doped single layer triangular antiferromagnet have been evaluated by considering the holon-spinon interaction[13,14]. According to these discussions, we obtain the full holon and spinon Green's functions of the doped bilayer triangular antiferromagnet by the loop expansion to the second-order as,

$$g^{-1}(k,\omega) = g^{(0)-1}(k,\omega) - \Sigma^{(h)}(k,\omega), \tag{9a}$$

$$D^{-1}(k,\omega) = D^{(0)-1}(k,\omega) - \Sigma^{(s)}(k,\omega), \tag{9b}$$

where $\Sigma^{(h)}(k,\omega) = \Sigma_L^{(h)}(k,\omega) + \sigma_x\Sigma_T^{(h)}(k,\omega)$ is the second-order holon self-energy from the spinon pair bubble, with the longitudinal and transverse parts are obtained as,

$$\Sigma_L^{(h)}(k,\omega) = \frac{1}{N^2}\sum_{pq}\sum_{\nu\nu'\nu''}\Xi^{(h)}_{\nu\nu'\nu''}(k,p,q,\omega), \tag{10a}$$

$$\Sigma_T^{(h)}(k,\omega) = \frac{1}{N^2}\sum_{pq}\sum_{\nu\nu'\nu''}(-1)^{\nu+\nu'+\nu''+1} \times \Xi^{(h)}_{\nu\nu'\nu''}(k,p,q,\omega), \tag{10b}$$

respectively, and $\Sigma^{(s)}(k,\omega) = \Sigma_L^{(s)}(k,\omega) + \sigma_x\Sigma_T^{(s)}(k,\omega)$ is the second-order spinon self-energy from the holon pair bubble, with the longitudinal and transverse parts are obtained as,

$$\Sigma_L^{(s)}(k,\omega) = \frac{1}{N^2}\sum_{pp'}\sum_{\nu\nu'\nu''}\Xi^{(s)}_{\nu\nu'\nu''}(k,p,p',\omega), \tag{11a}$$

$$\Sigma_T^{(s)}(k,\omega) = \frac{1}{N^2}\sum_{pp'}\sum_{\nu\nu'\nu''}(-1)^{\nu+\nu'+\nu''+1} \times \Xi^{(s)}_{\nu\nu'\nu''}(k,p,p',\omega), \tag{11b}$$

respectively, where

$$\Xi^{(h)}_{\nu\nu'\nu''}(k,p,q,\omega) = \frac{B^{(\nu')}_{q+p}B^{(\nu)}_{q}}{32\omega^{(\nu')}_{q+p}\omega^{(\nu)}_{q}}\left(Zt_{\parallel}[\gamma_{q+p+k}+\gamma_{q-k}] + t_{\perp}[(-1)^{\nu+\nu''}+(-1)^{\nu'+\nu''}]\right)^2 \times\left(\frac{F^{(1)}_{\nu\nu'\nu''}(k,p,q)}{\omega+\omega^{(\nu')}_{q+p}-\omega^{(\nu)}_{q}-\xi^{(\nu'')}_{p+k}} + \frac{F^{(2)}_{\nu\nu'\nu''}(k,p,q)}{\omega-\omega^{(\nu')}_{q+p}+\omega^{(\nu)}_{q}-\xi^{(\nu'')}_{p+k}} + \frac{F^{(3)}_{\nu\nu'\nu''}(k,p,q)}{\omega+\omega^{(\nu')}_{q+p}+\omega^{(\nu)}_{q}-\xi^{(\nu'')}_{p+k}} + \frac{F^{(4)}_{\nu\nu'\nu''}(k,p,q)}{\omega-\omega^{(\nu')}_{q+p}-\omega^{(\nu)}_{q}-\xi^{(\nu'')}_{p+k}}\right), \tag{12a}$$

$$\Xi^{(s)}_{\nu\nu'\nu''}(k,p,p',\omega) = \frac{B^{(\nu'')}_{k+p}}{16\omega^{(\nu'')}_{k+p}}\left(Zt_{\parallel}[\gamma_{p'+p+k}+\gamma_{k-p'}] + t_{\perp}[(-1)^{\nu'+\nu''}+(-1)^{\nu+\nu''}]\right)^2 \times\left(\frac{L^{(1)}_{\nu\nu'\nu''}(k,p,p')}{\omega+\xi^{(\nu')}_{p+p'}-\xi^{(\nu)}_{p'}-\omega^{(\nu'')}_{k+p}} - \frac{L^{(2)}_{\nu\nu'\nu''}(k,p,p')}{\omega+\xi^{(\nu')}_{p+p'}-\xi^{\nu}_{p'}+\omega^{(\nu'')}_{k+p}}\right), \tag{12b}$$

with

$$F^{(1)}_{\nu\nu'\nu''}(k,p,q) = n_F(\xi^{(\nu'')}_{p+k})[n_B(\omega^{(\nu)}_{q}) - n_B(\omega^{(\nu')}_{q+p})] + n_B(\omega^{(\nu')}_{q+p})[1+n_B(\omega^{(\nu)}_{q})], \tag{13a}$$

$$F^{(2)}_{\nu\nu'\nu''}(k,p,q) = n_F(\xi^{(\nu'')}_{p+k})[n_B(\omega^{(\nu')}_{q+p}) - n_B(\omega^{(\nu)}_{q})] + n_B(\omega^{(\nu)}_{q})[1+n_B(\omega^{(\nu')}_{q+p})], \tag{13b}$$

$$F^{(3)}_{\nu\nu'\nu''}(k,p,q) = n_F(\xi^{(\nu'')}_{p+k})[1+n_B(\omega^{(\nu')}_{q+p}) + n_B(\omega^{(\nu)}_{q})] + n_B(\omega^{(\nu)}_{q})n_B(\omega^{(\nu')}_{q+p}), \tag{13c}$$

$$F^{(4)}_{\nu\nu'\nu''}(k,p,q) = [1+n_B(\omega^{(\nu)}_{q})][1+n_B(\omega^{(\nu')}_{q+p})] - n_F(\xi^{(\nu'')}_{p+k})[1+n_B(\omega^{(\nu')}_{q+p}) + n_B(\omega^{(\nu)}_{q})], \tag{13d}$$

$$L^{(1)}_{\nu\nu'\nu''}(k,p,p') = n_F(\xi^{(\nu')}_{p+p'})[1-n_F(\xi^{(\nu)}_{p'})] - n_B(\omega^{(\nu'')}_{k+p}) \times [n_F(\xi^{(\nu)}_{p'}) - n_F(\xi^{(\nu')}_{p+p'})], \tag{13e}$$

$$L^{(2)}_{\nu\nu'\nu''}(k,p,p') = n_F(\xi^{(\nu')}_{p+p'})[1-n_F(\xi^{(\nu)}_{p'})] + [1+n_B(\omega^{(\nu'')}_{k+p})] \times [n_F(\xi^{(\nu)}_{p'}) - n_F(\xi^{(\nu')}_{p+p'})], \tag{13f}$$

and $n_F(\xi^{(\nu)}_{k})$ and $n_B(\omega^{(\nu)}_{k})$ are the fermion and boson distribution functions, respectively. Within the fermion-spin theory, the spin fluctuation couples only to spinons, while the charge fluctuation couples only to holons[13,14], this is because that the local constraint with no doubly occupied has been treated properly, and therefore leads to disappearing of the extra gauge degree of freedom related with the local constraint under the charge-spin separation. However, the strong correlation between holons and spinons still is included self-consistently through the holon's order parameters entering the spinon's propagator and the spinon's order parameters entering the holon's propagator, therefore both holons and spinons are responsible for the optical, transport and magnetic behaviors.

III. CHARGE TRANSPORT

Among the striking features of the unusual physical properties stands out the extraordinary charge transport[1,2]. The frequency- and temperature-dependent conductivity is a powerful probe for systems of interacting electrons, and provides very detailed informations of the excitations, which interacts with carriers in the normal-state and might play an important role in the superconductivity. In the framework of the fermion-spin theory, the charge fluctuation couples only to holons as mentioned above, and therefore as in the doped single layer case[13], the conductivity of the doped bilayer triangular antiferromegnet is obtained as,

$$\sigma(\omega) = -\frac{\mathrm{Im}\Pi^{(h)}(\omega)}{\omega}, \tag{14}$$

where $\Pi^{(h)}(\omega)$ is the holon current-current correlation function, and is defined as $\Pi^{(h)}(\tau - \tau') = -\langle T_\tau j^{(h)}(\tau) j^{(h)}(\tau')\rangle$, with τ and τ' are the imaginary times, and T_τ is the τ order operator. Within the Hamiltonian (3), the current density of holons is obtained by the time derivation of the polarization operator using Heisenberg's equation of motion as,

$$j^{(h)} = 2\chi_\parallel e t_\parallel \sum_{ai\hat{\eta}} \hat{\eta} h^\dagger_{ai+\hat{\eta}} h_{ai} + 2\chi_\perp e t_\perp \sum_i (R_{2i} - R_{1i})(h^\dagger_{2i} h_{1i} - h^\dagger_{1i} h_{2i}), \tag{15}$$

where R_{1i} (R_{2i}) is the lattice site of the plane 1 (plane 2), and e is the electronic charge, which is set as the unit hereafter. This holon current-current correlation function can be calculated in terms of the full holon Green's function $g(k,\omega)$. After a straightforward calculation, we obtain explicitly the conductivity of the doped bilayer triangular antiferromagnet as,

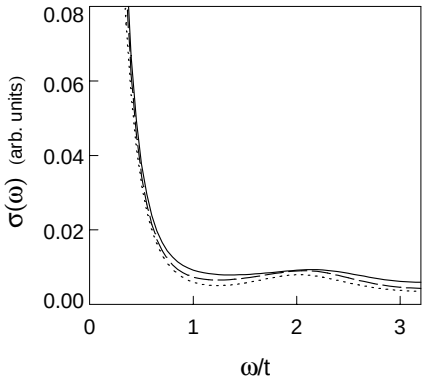

FIG. 1. The conductivity at $x = 0.12$ (solid line), $x = 0.09$ (dashed line), and $x = 0.06$ (dotted line) in $T = 0$ for $t_\parallel/J_\parallel = 2.5$, $t_\perp/t_\parallel = 0.25$, and $J_\perp/J_\parallel = 0.25$.

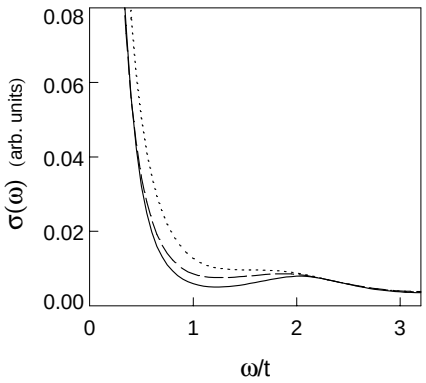

FIG. 2. The conductivity in $T = 0$ (solid line), $T = 0.3J_\parallel$ (dashed line), $T = 0.5J_\parallel$ (dotted line) at $x = 0.06$ for $t_\parallel/J_\parallel = 2.5$, $t_\perp/t_\parallel = 0.25$, and $J_\perp/J_\parallel = 0.25$.

$$\sigma(\omega) = \sigma^{(L)}(\omega) + \sigma^{(T)}(\omega), \tag{16}$$

with the longitudinal and transverse parts are given by,

$$\sigma^{(L)}(\omega) = \frac{1}{N}\sum_k [(2Z\chi_\parallel t_\parallel \gamma_{sk})^2 + (2\chi_\perp t_\perp)^2] \times \int_{-\infty}^{\infty} \frac{d\omega'}{2\pi} A_L^{(h)}(k,\omega'+\omega) A_L^{(h)}(k,\omega') \times \frac{n_F(\omega'+\omega) - n_F(\omega')}{\omega}, \tag{17a}$$

$$\sigma^{(T)}(\omega) = \frac{1}{N}\sum_k [(2Z\chi_\parallel t_\parallel \gamma_{sk})^2 - (2\chi_\perp t_\perp)^2] \times \int_{-\infty}^{\infty} \frac{d\omega'}{2\pi} A_T^{(h)}(k,\omega'+\omega) A_T^{(h)}(k,\omega') \times \frac{n_F(\omega'+\omega) - n_F(\omega')}{\omega}, \tag{17b}$$

respectively,
where $\gamma^2_{sk} = [\sin(k_x) + \sin(k_x/2)\cos(\sqrt{3}k_y/2)]^2/9 + [\cos(k_x/2)\sin(\sqrt{3}k_y/2)]^2/3$, $A_L^{(h)}(k,\omega) = -2\mathrm{Im}g_L(k,\omega)$ and $A_T^{(h)}(k,\omega) = -2\mathrm{Im}g_T(k,\omega)$ are the holon's longitudinal and transverse spectral functions.

In Fig. 1, we present the conductivity at doping $x = 0.12$ (solid line), $x = 0.09$ (dashed line), and $x = 0.06$ (dotted line) for parameters $t_\parallel/J_\parallel = 2.5$, $t_\perp/t_\parallel = 0.25$, and $J_\perp/J_\parallel = 0.25$ in temperature $T = 0$, where $\sigma(\omega)$ shows a sharp low-energy peak and the unusual mid-infrared band separated by the charge-transfer gap of the undoped system. This low-energy peak decays fastly with increasing energy, while the charge-transfer gap is

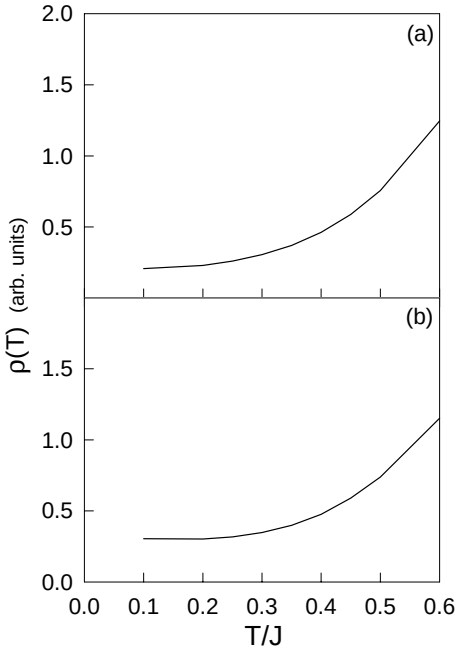

FIG. 3. The resistivity at (a) $x = 0.12$ and (b) $x = 0.06$ for $t_\parallel/J_\parallel = 2.5$, $t_\perp/t_\parallel = 0.25$, and $J_\perp/J_\parallel = 0.25$.

doping dependent, deceases with increasing dopings, and vanishes in higher doped regime. For the better understanding of the optical properties, we also study the conductivity at different temperatures and the results in $T = 0$ (solid line), $T = 0.3J_{\parallel}$ (dashed line), and $T = 0.5J_{\parallel}$ (dotted line) at $x = 0.06$ for $t_{\parallel}/J_{\parallel} = 2.5$, $t_{\perp}/t_{\parallel} = 0.25$, and $J_{\perp}/J_{\parallel} = 0.25$ are shown in Fig. 2. We therefore find that the charge-transfer gap also decreases with increasing temperature, and disappears at higher temperatures. In the above calculations, we also find that the conductivity $\sigma(\omega)$ of the doped bilayer triangular antiferromagnet is essentially determined by its longitudinal part $\sigma^{(L)}(\omega)$, this is why in the present bilayer system the conductivity spectrum appears to reflect the single layer nature of the electronic state[13].

Now we turn to discuss the resistivity. The resistivity is closely related to the conductivity, and can be obtained as $\rho(T) = 1/\lim_{\omega\rightarrow 0}\sigma(\omega)$. We have performed the calculation for $\rho(T)$, and the results at $x = 0.12$ and $x = 0.06$ for $t_{\parallel}/J_{\parallel} = 2.5$, $t_{\perp}/t_{\parallel} = 0.25$, and $J_{\perp}/J_{\parallel} = 0.25$ are plotted in the Fig. 3(a) and Fig. 3(b), respectively. These results show that the temperature-dependent resistivity of the doped bilayer triangular antiferromagnet is characterized by the nonlinearity metallic-like behavior in the higher temperature range, and the deviation from the metallic-like behavior in the lower temperature range. In comparison with the results of the doped singlar triangular antiferromagnet[13], it is shown that although the bilayer interaction leads to the band splitting in the electronic structure, the qualitative behavior of the charge transport is the same as in the single layer case.

Since the t-J model is characterized by the competition between the kinetic energy (t) and magnetic energy (J). The magnetic energy J favors the magnetic order for spins, while the kinetic energy t favors delocalization of holes and tends to destroy the magnetic order. In the present fermion-spin theory, although both holons and spinons contribute to the charge transport, the scattering of holons dominates the charge transport, where the charged holon scattering rate is obtained from the full holon Green's function (then the holon self-energy (10) and holon spectral function) by considering the holon-spinon interaction. In this case, the unusual behavior in the resistivity is closely related with this competition. In the underdoped regime, the holon kinetic energy is much smaller than the magnetic energy in lower temperatures, therefore the magnetic fluctuation is strong enough to heavily reduce the charged holon scattering and thus is responsible for the deviation from the metallic-like behavior in the resistivity. With increasing temperatures, the holon kinetic energy is increased, while the spinon magnetic energy is decreased. In the region where the holon kinetic energy is much larger than the spinon magnetic energy at high temperatures, the charged holon scattering would give rise to the metallic-like behavior in the resistivity.

IV. SPIN RESPONSE

The antiferromagnetic spin correlation is responsible for the nuclear magnetic resonance (NMR), nuclear quadrupole resonance (NQR), and especially for the temperature dependence of the spin-lattice relaxation rate[1,2]. This spin response is manifested by the dynamical spin structure factor $S(k,\omega)$, which can be obtained in the present bilayer triangular antiferromagnet as,

$$S(k,\omega) = -2[1+n_B(\omega)][2\mathrm{Im}D_L(k,\omega)+2\mathrm{Im}D_T(k,\omega)] = -\frac{4[1+n_B(\omega)](B_k^{(1)})^2\mathrm{Im}\Sigma_{LT}^{(s)}(k,\omega)}{A+B}, \qquad (18)$$

where $A = [\omega^2 - (\omega_k^{(1)})^2 - B_k^{(1)}\mathrm{Re}\Sigma_{LT}^{(s)}(k,\omega)]^2$, $B = [B_k^{(1)}\mathrm{Im}\Sigma_{LT}^{(s)}(k,\omega)]^2$, and $\mathrm{Im}\Sigma_{LT}^{(s)}(k,\omega) = \mathrm{Im}\Sigma_{L}^{(s)}(k,\omega) + \mathrm{Im}\Sigma_{T}^{(s)}(k,\omega)$ and $\mathrm{Re}\Sigma_{LT}^{(s)}(k,\omega) = \mathrm{Re}\Sigma_{L}^{(s)}(k,\omega) + \mathrm{Re}\Sigma_{T}^{(s)}(k,\omega)$, while $\mathrm{Im}\Sigma_{L}^{(s)}(k,\omega)$ ($\mathrm{Im}\Sigma_{T}^{(s)}(k,\omega)$) and $\mathrm{Re}\Sigma_{L}^{(s)}(k,\omega)$ ($\mathrm{Re}\Sigma_{T}^{(s)}(k,\omega)$) are the imaginary and real parts of the second order longitudinal (transverse) spinon self-energy (11), respectively.

In Fig. 4, we present the result of the dynamical spin structure factor $S(k,\omega)$ in the (k_x,k_y) plane at (a) $x = 0.02$ and (b) $x = 0.06$ in $T = 0.1J_{\parallel}$ and $\omega = 0.05J_{\parallel}$ for $t_{\parallel}/J_{\parallel} = 2.5$, $t_{\perp}/t_{\parallel} = 0.2$, and $J_{\perp}/J_{\parallel} = 0.2$, hereafter we use the units of $[2\pi/3, 2\pi/3]$. Obviously, there is a commensurate-incommensurate transition in the spin fluctuation with dopings. Near the half-filling, the spin

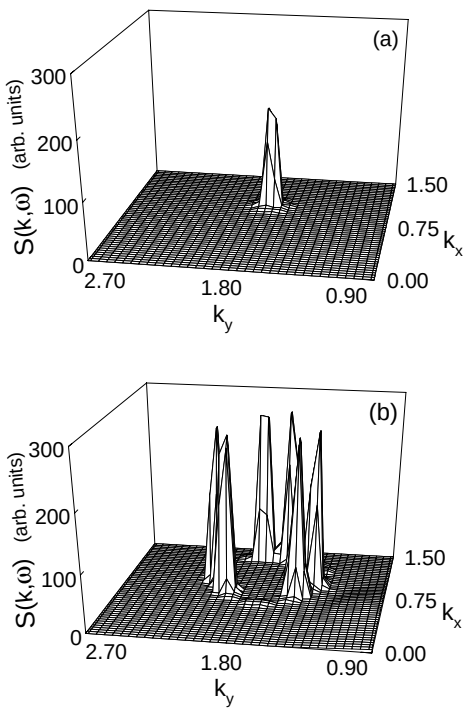

FIG. 4. The dynamical spin structure factor in the (k_x,k_y) plane at (a) $x = 0.02$ and (b) $x = 0.06$ in $T = 0.1J_{\parallel}$ and $\omega = 0.05J_{\parallel}$ for $t_{\parallel}/J_{\parallel} = 2.5$, $t_{\perp}/t_{\parallel} = 0.2$, and $J_{\perp}/J_{\parallel} = 0.2$.

fluctuation is commensurate, and the position of the commensurate neutron scattering peak is located at the antiferromagnetic wave vector $\mathbf{Q} = [1, \sqrt{3}]$. However, this commensurate peak is split into six peaks in the underdoped regime, while the positions of these incommensurate peaks are located at $[(1-\delta_x), (\sqrt{3} \pm \delta_y)]$, $[(1-\delta'_x), (\sqrt{3} \pm \delta'_y)]$, and $[(1-\delta''_x), (\sqrt{3} \pm \delta''_y)]$, with $\sqrt{\delta_x^2 + \delta_y^2} = \sqrt{(\delta'_x)^2 + (\delta'_y)^2} = \sqrt{(\delta''_x)^2 + (\delta''_y)^2} = \delta$. The calculated dynamical spin structure factor spectrum has been used to extract the doping dependence of the incommensurability parameter $\delta(x)$, defined as the deviation of the peak position from the antiferromagnetic wave vector $\mathbf{Q}$, and the result is plotted in Fig. 5, where $\delta(x)$ increases with the hole concentration in lower dopings, but it saturates at higher dopings, and is qualitatively similar to the results of the doped single layer triangular antiferromagnet[14]. For the further understanding of the magnetic properties, we have made a series of scans for $S(k, \omega)$ at different temperatures and energies, and find that as in the single layer case, the weight of the incommensurate peaks are broadened and suppressed with increasing temperatures. Moreover, although the positions of the incommensurate peaks are almost energy independent, the weight of these peaks decreases with increasing energy, and tends to vanish at high energies. This reflects that the inverse lifetime of the spin excitations increases with increasing energy.

The physical origin of the incommensurate magnetic fluctuation in the doped bilayer triangular antiferromagnet is the almost same as in the single layer case[14], and is induced by the spinon self-energy renormalization due to holons, *i.e.*, the mechanism of the incommensurate type of structure away from the half-filling is most likely related to the holon motion. $S(\mathbf{k}, \omega)$ in Eq. (18) exhibits peaks when the incoming neutron energy ω is equal to the renormalized spin excitation $E_k^2 = (\omega_k^{(1)})^2 + B_k^{(1)} \mathrm{Re}\Sigma_{LT}^{(s)}(k, E_k)$, *i.e.*, $[\omega^2 - (\omega_{k_c}^{(1)})^2 - B_{k_c}^{(1)} \mathrm{Re}\Sigma_{LT}^{(s)}(k_c, \omega)]^2 = (\omega^2 - E_{k_c}^2)^2 \sim 0$ for certain critical wave vectors $\mathbf{k}_c$. The height of these peaks then is determined by the imaginary part of the spinon self-energy $1/\mathrm{Im}\Sigma_{LT}^{(s)}(k_c, \omega)$. This renormalized spin excitation is doping and temperature dependent. Near half-filling, the spin excitations are centered around the antiferromagnetic wave vector $\mathbf{Q}$, so the commensurate antiferromagnetic peak appears there. Upon doping, the holes disturb the antiferromagnetic background. Within the fermion-spin framework, as a result of self-consistent motion of holons and spinons, the incommensurate antiferromagnetism is developed beyond certain critical doping, which means that the low-energy spin excitations drift away from the antiferromagnetic wave vector, where the physics is dominated by the spinon self-energy $\mathrm{Re}\Sigma_L^{(s)}(k, \omega)$ renormalization due to holons. This is why the mobile holes are the key factor leading to the incommensurate antiferromagnetism, while the spinon energy dependence is ascribed purely to self-energy effects which arise from the holon-spinon interaction. Since the height of the incommensurate peaks is determined by damping, it is fully understandable that they are suppressed as the neutron energy ω and temperature are increased.

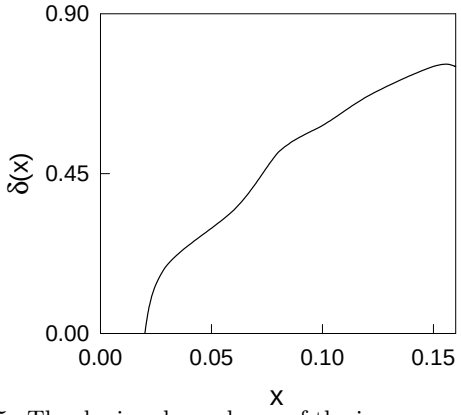

FIG. 5. The doping dependence of the incommensurability $\delta(x)$ of the antiferromagnetic fluctuations.

V. SUMMARY AND DISCUSSIONS

In the above discussions, the central concern of the charge transport and spin response in the doped bilayer triangular antiferromagnet is the quasi-two dimensionality of the electron state, then the charge transport is mainly determined by the longitudinal charged holon fluctuation, and spin response is dominated by the longitudinal spinon fluctuation. On the other hand, our present study also indicates that the physical properties of the doped antiferromagnet are heavily dependent on the electron geometry structure. Unlike the doped square antiferromagnet, the resistivity in the doped triangular antiferromagnet does not exhibits a linear metallic-like behavior in the higher temperature range as would be expected for the doped square antiferromagnet, while six incommensurate neutron scattering peaks in the doped triangular antiferromagnet are incompatible with these in the doped square antiferromagnet, where four incommensurate peaks are observed[5,6].

In summary, we have discussed the charge transport and spin response of the doped bilayer triangular antiferromagnet within the framework of the fermion-spin theory based on the t-J model. It is shown that although the bilayer interaction leads to the band splitting in the electronic structure, the qualitative behaviors of the charge transport and spin response are the same as in the single layer case[13,14]. The conductivity spectrum shows the low-energy peak and unusual midinfrared band separated by the charge-transfer gap, while the temperature dependent resistivity is characterized by the nonlinearity metallic-like behavior in the higher temperature range, and the deviation from the metallic-like behavior in the lower temperature range. The commensurate neutron

scattering peak near the half-filling is split into six incommensurate peaks in the underdoped regime, with the incommensurability increases with the hole concentration at lower dopings, and saturates at higher dopings.

ACKNOWLEDGMENTS

The authors would like to thank Feng Yuan and Jihong Qin for helpful discussions. This work was supported by the National Natural Science Foundation of China, and the special funds from the Ministry of Science and Technology of China.

[1] See, *e.g.*, *Physical Properties of High Temperature Superconductors*, edited by D.M. Ginsberg (World Scientific, Singapore, 1994).

[2] See, *e.g.*, *Proceedings of Los Alamos Symposium*, edited by K.S. Bedell, D. Coffey, D.E. Meltzer, D. Pines, and J.R. Schrieffer (Addison-Wesley, Redwood city, California, 1990).

[3] T. Ito, K. Takenaka, and S. Uchida, Phys. Rev. Lett. **70**, 3995 (1993); S. Uchida, Physica C**282-287**, 12 (1997).

[4] P.W. Anderson, in *Frontiers and Borderlines in Many Particle Physics*, edited by R.A. Broglia and J.R. Schrieffer (North-Holland, Amsterdam, 1987), p. 1; Science **235**, 1196 (1987).

[5] K. Yamada, C.H. Lee, K. Kurahashi, J. Wada, S. Wakimoto, S. Ueki, H. Kimura, Y. Endoh, S. Hosoya, and G. Shirane, Phys. Rev. B **57**, 6165 (1998), and references therein.

[6] P. Dai, H.A. Mook, R.D. Hunt, and F. Doğan, Phys. Rev. B**63**, 54525 (2001), and references therein.

[7] O.K. Anderson, A.I. Liechtenstein, O. Jepsen, and F. Paulsen, J. Phys. Chem. Solids **56**, 1573 (1995); A.I. Liechtenstein, O. Gunnarsson, O.K. Anderson, and R.M. Martin, Phys. Rev. B**54**, 12505 (1996).

[8] D.L. Feng, N.P. Armitage, D.H. Lu, A. Damascelli, J.P. Hu, P. Bogdanov, A. Lanzara, F. Ronning, K.M. Shen, H. Eisaki, C. Kim, Z.X. Shen, J.-i. Shimoyama, and K. Kishio, Phys. Rev. Lett. **86**, 5550 (2001).

[9] Y.-D. Chuang, A.D. Gromko, A.V. Fedorov, Y. Aiura, K. Oka, Yoichi Ando, and D. Dessau, cond-mat/0107002; Y.-D. Chuang, A.D. Gromko, A.V. Fedorov, Y. Aiura, K. Oka, Yoichi Ando, H. Eisaki, S.I. Uchida, and D. Dessau, Phys. Rev. Lett. **87**, 117002 (2001).

[10] A.P. Ramirez, R.J. Cava, J.J. Krajewski, and W.F. Peck, Jr., Phys. Rev. B **49**, 16082 (1994); R.J. Cava, H.W. Zandbergen, A.P. Ramirez, H. Takagi, C.T. Chen, J.J. Krajewski, W.F. Peck, Jr., J.V. Waszczak, G. Meigs, and L.F. Schneemeyer, J. Solid State Chem. **104**, 437 (1993).

[11] M. Azuma, T. Odaka, M. Takano, D.A. Vander Griend, K.R. Poeppelmeier, Y. Narumi, K. Kindo, Y. Mizuno, and S. Maekawa, Phys. Rev. B **62**, R3588 (2000).

[12] M. Uehara, T. Nagata, J. Akimitsu, H. Takahashi, N. Mori, and K. Kinoshita, J. Phys. Soc. Jpn. **65**, 2764 (1996).

[13] W.Q. Yu, Shiping Feng, Z.B. Huang and H.Q. Lin, Phys. Rev. B **61**, 7409 (2000).

[14] Ying Liang and Shiping Feng, Phys. Lett. A **296**, 301 (2002).

[15] P.W. Anderson, Mater. Res. Bull, **8**, 153 (1973); P. Fazekas and P.W. Anderson, Philos. Mag. **30**, 423 (1974).

[16] R.B. Laughlin, Phys. Rev. Lett. **60**, 2677 (1988); M. Vojta and E. Dagotto, Phys. Rev. B **59**, R713 (1999).

[17] Shiping Feng, Z.B. Su, and L. Yu, Phys. Rev. B **49**, 2368 (1994); Mod. Phys. Lett. B **7**, 1013 (1993).

[18] L. Caprioti, A. E. Trumper, and S. Sorella, Phys. Rev. Lett. **82**, 3899 (1999).

[19] Shiping Feng and Yun Song, Phys. Rev. B **55**, 642 (1997).